



NJC

Highly Dispersible Silica pH Nanosensor with Expanding Measurement Range

Journal:	<i>New Journal of Chemistry</i>
Manuscript ID:	NJ-ART-12-2014-002419.R1
Article Type:	Paper
Date Submitted by the Author:	17-Mar-2015
Complete List of Authors:	Hu, Shuchao; Hubei university of teachnology, ; Sun, Ling; Hubei university of teachnology, Sun, Honghao; Hubei university of teachnology, Liu, Mingxing; Hubei university of teachnology, Zhu, Hongda; Hubei university of teachnology, Guo, Huiling; Hubei university of teachnology, Sun, Hongmei; Hubei university of teachnology,

SCHOLARONE™
Manuscripts

ARTICLE

Highly Dispersible Silica pH Nanosensor with Expanding Measurement Range

Cite this: DOI: 10.1039/x0xx00000x

Shuchao Hu, Ling Sun, Mingxing Liu, Hongda Zhu, Huiling Guo, Hongmei Sun and Honghao Sun*

Received 00th January 2012,
Accepted 00th January 2012

DOI: 10.1039/x0xx00000x

www.rsc.org/

For accurate determination of local intracellular pH which could further improve our understanding of cellular processes and knowledge of advanced drug delivery systems architect, fluorescent-based ratiometric nanosensor has been designed over the past decade. As a promising matrix for nanosensor and nanomedicine, silica nanoparticles (SNP) have been widely used due to the desirable properties which include high loading level of guest molecules, low toxicity and easy functionalization. Amination of SNP was essential for binding functional groups, such as fluorescent molecule, targeting group, whereas positive charged amine will cause the aggregation of SNP which limits the further application of SNP. To circumvent this problem, a simple and effective strategy has been presented in this paper. Firstly, acid was used as catalyst instead of base to inhibit the SNP aggregation in amination process. Subsequently, polymers (poly (ethylene glycol) and hyaluronic acid) were coated on surface of monodispersed aminated SNP to obtain excellent colloidal stability. The well dispersed core-shell SNP were further functionalized with two pH sensitive fluorophore (fluorescein isothiocyanate and Oregon Green isothiocyanate) and one reference fluorophore (rhodamine B isothiocyanate), which resulted in ratiometric pH nanosensors with hydrodynamic diameter of 76-100nm. The sensors exhibited broad pH measurement range from 3.8 to 7.4 that covers almost all intracellular pH values and remarkable colloidal stability in buffer solution.

Introduction

Intracellular pH plays a pivotal role in organelles such as lysosomes and mitochondria, as well as in cell cycle progression and apoptosis.¹⁻⁴ Consequently, accurate determination of local intracellular pH in organelles of living cells is essential for increasing our understanding of cellular processes. Furthermore, great deals of advanced drug delivery systems are designed to be pH-sensitive by providing structural changes to drug release in response to decrease in pH after endocytosis and during intracellular trafficking to lysosomes.⁵⁻

¹¹ However, there is very limited knowledge on the intracellular trafficking of these systems, particularly regarding the pH that the particles are experiencing after internalization. At present, it is just assumed that the pH-sensitive drug delivery system ends

up in acidic compartments, but this hasn't been tested. Thus, nanoparticle pH sensors could play an important role in enhancing our basic understanding of nanoparticle internalization mechanisms and the cellular environment a nanoparticle experiences after internalization, which could further improve our understanding of how to design better drug delivery systems that release their cargo in a controlled manner as a response to acidification in the surroundings.

A number of ratio metric fluorescence method based nanosensors have been developed in the last decade for intracellular pH measurement by various groups.¹²⁻¹⁶ Generally, this method is based on the intensity ratio of the emission peaks from the pH sensitive dye and the reference dye that were covalently bounded to the carrier. A triple fluorophore labelled

polyacrylamide nanosensor with a broad measurement range was prepared by reverse microemulsion polymerization.¹⁵ During this process tedious freeze-vacuum-thaw was repeated at least four times to remove the dissolved oxygen. Large amount of surfactant and organic solvent were also involved. In addition, the degradation of polyacrylamide would induce the leakage of fluorescent molecules and generate cytotoxic and cancerogenic oligomer.¹⁷

Silica nanoparticles (SNP) possessing easy fabrication, large surface area, low toxicity and easy functionalization properties have been widely used as the matrix for biological application.¹⁹⁻²⁵ To study the pH environment after SNP nanomedicine were internalized in cells, SNP based pH sensor was developed. Mou and co-workers²⁵ reported a fluorescent pH sensor based on mesoporous silica nanoparticles (MSN) and hollow mesoporous silica (HMSN) with expanded pH measurement ranges (pH response ranges are 4.7-7.0 and 4.5-8.5 respectively), but the positive potential (26mv and 30mv respectively) would induce some unexpected interactions with the negative proteins and cytomembrane.²⁶ Additionally, exposure to naked SNP can significantly reduce the cell viability in a dose-dependent and time-dependant manner.²⁷ Although the SNP is frequently reported as a matrix for biosensing or drug delivering, naked or aminated SNP tended to be aggregated in buffer, and the dried SNP was even unable to be dispersed.²⁸⁻³⁰ The results in our work also confirm this suggestion. Brinker and co-workers reported that the vast majority of dried SNP were undispersible, only a few of particles were remained after purification by size exclusion-based separation. These SNP were encapsulated into liposomes to enhance their colloidal stability and cargo retention in simulated body fluids and minimize nonspecific interactions with serum proteins and non-cancerous cells.²⁸ But the structure was not stable enough for biodetection, because the lipid bilayer may be fused with cell membrane in the process of cellular internalization.³⁰ To obtain sufficient colloidal and structural stability, poly (ethylene glycol) (PEG)-grafted colloidal SNP were presented by Zhang and Buitenhuis.³¹ However, the complicated procedure of gel permeation chromatography needed to be performed for ammonium and residual silane oligomers removing.

In the present paper, a simple method was used to prepare well dispersed SNP which was further functionalized with

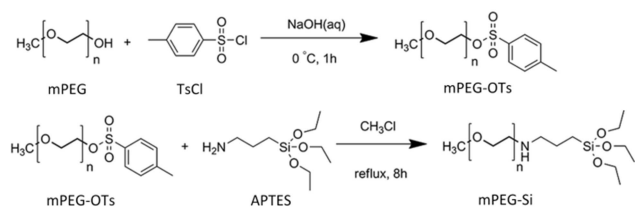
fluorophore for pH values determination. The preparation procedure of SNP pH nanosensors can be described by three steps, amination, polymer coating and dyes conjugating. The amination of SNP was necessary for functional group conjugating, whereas the procedure of amination which was carried out *in situ* at the end of the Stöber synthesis would lead to a strong particle aggregation.³²⁻³⁵ Even after conjugated with water soluble polymer, the white precipitate was still unable to disperse. In this paper, amination of SNP was carried out in acid environment instead of basic environment. SNP aggregation can be effectively eliminated. Two polymers, mPEG and hyaluronic acid (HA), were used for SNP coating. PEGylation and HA modification can greatly enhanced the biostability and biocompatibility of particles.³⁶⁻³⁹ After the polymer coated SNP were simply washed for several times with water and ethanol, the particles can be stably dispersed in buffer. Large scale well dispersed SNP could be prepared by this simple method. HA could also act as a ligand for Cluster Determinant 44 (CD44) which is overexpressed in several cancer types.⁴¹⁻⁴² Additionally, the intracellular transport of this rigidity particle can be monitored because of the fluorescence, which could provide a new insight into drug delivery process of SNP based nanomedicine.

Experimental

Materials

Tetraethyl orthosilicate (TEOS), Tetrahydrofuran (THF), NaOH, ammonia solution(25%), HCl (conc.), chloroform, MgSO₄, N-hydroxysuccinimidyl (NHS) (95%-99%) were purchased from Sinopharm Chemical Reagent Co., Ltd. Sodium hyaluronate (Mw=66000), Aminopropyl triethoxysilane (APTES) (97%), p-toluenesulfonyl chloride (TsCl) (99%) were purchased from Aladdin Chemistry Co. (Shanghai). 1-ethyl-3-(3-dimethylaminopropyl)-carbodiimide hydrochloride (EDC·HCl) (99%) was purchased from Shanghai Medpep Co., Ltd. Oregon Green isothiocyanate (OG) was purchased from Invitrogen. Methoxypolyethylene glycols (mPEG, MW=5000), Rhodamine B isothiocyanate (RhB), Fluorescein isothiocyanate (FS) were purchased from Sigma-Aldrich. All the chemicals were analytical grade and used without further treatment.

Synthesis of PEG-silane Precursor (mPEG-Si)



Scheme 1 The synthesis of PEG-silane precursor with Mw 5000.

PEG-silane precursor was synthesized as shown in Scheme 1. 20g (4.0 mmol) of mPEG (Mw =5000) in 10 mL THF were added to a solution of 800 mg (20 mmol) NaOH in 40 mL Milli-Q water. The resulting mixture was stirred for 1 h at 0°C. Then 1 g (5.2 mmol) TsCl in 10 mL THF was added drop wise to the reaction mixture during 1 h at 0°C. After the mixture was stirred for another 3 h at r.t, the solution was poured into 20 mL 1 M HCl in beakers and the organic solvent was evaporated in vacuum. The residue was extracted with 25 mL chloroform for 3 times, and the organic phase was dried over MgSO₄, followed by filtration and the solvent was removed by rotary evaporation. The transparent crude product was reacted with 1mL (4.3mmol, slightly excess) APTES in 25 mL chloroform for 8 h under reflux conditions. The organic solvent was removed by rotary evaporation to obtain the raw product. The product was precipitated three times with cold ether and dried under vacuum to give 17g (81% yields) mPEG-Si which was stored at 4°C.

Preparation of SNP

SNP were prepared according to Stöber method.³² 0.8 mL ammonia solution was added to 25 mL ethanol at room temperature under vigorous stirring. After mixing for 5 min, 1 mL of TEOS was added and the reaction mixture was allowed to react for 24 h. The ammonia and oligomers were removed by centrifugation at 15000rpm for 30 min, and the residue was dispersed in 20 mL ethanol.

Amination of SNP

200 µL of APTES (20% of TEOS) and 200 µL Milli-Q water was added into SNP suspension at 60°C and continued to stir for 5min. The solution changed from transparent to turbid. Then 1mL acetate acid was added to eliminate the aggregation and catalyse the hydrolytic condensation. After stirring at r.t for 3 hours, the reaction mixture changed to transparent again, with no sign of aggregation. The SNP-NH₂ was collected by

centrifugation at 15000rpm for 30 min and purified by washing with ethanol and water for several times. Finally, the sample was dispersed in 20mL Milli-Q water.

PEGylation of SNP

10mL Si-PEG aqueous solution (15mg/mL) was added to 10 mL of SNP-NH₂ aqueous suspension (15mg/mL), the resulting mixture was stirred overnight. The nanoparticles were collected by centrifugation at 13000rpm for 30 min. SNP-NH₂-PEG₅₀₀₀ solid was washed with water and ethanol for at least for 5 times. Finally, the solid was dispersed in Milli-Q water and kept at 4 °C.

HA Coating of SNP

30 mg EDC was added to 15 mL of HA aqueous solution (containing 60 mg HA) and stand for 15 min, followed by adding 20 mg NHS. Then the mixed solution was added into 10 mL of SNP-NH₂ suspension (15mg/mL, acidized by 1M HCl, pH=2). The mixture was stirred for 12 h at r.t followed by dialyzing against Milli-Q water for 4 days (4 times water change) using cellulose dialysis tubing (MW cutoff 300 kDa) to remove free HA, EDC, and NHS.

Preparation of SNP-OG-FS-RhB-PEG and SNP-OG-FS-RhB-HA

The primary amino groups in the SNPs were used to conjugate the pH sensitive dyes. 300 µL of NaHCO₃/Na₂CO₃ buffer (0.2 M, pH 9.2) was added to 5 mL of SNP-PEG aqueous solution (50 mg/mL) to deprotonate the primary amine, followed by adding 83 µL FS (1 mg/mL in DMSO), 99 µL OG (1 mg/mL in DMSO), and 175 µL RhB (1 mg/mL in DMSO) to the SNPs solution. The reaction mixture was stirred for 4 h and was dialyzed against Milli-Q water for 4 days using cellulose dialysis tubing (MW cutoff 10 kDa) to remove any free fluorophore and DMSO. SNP-OG-FS-RhB-HA was synthesized in the same procedure.

pH Calibration Curve from Spectrofluorometer

The pH calibration curve was constructed by fluorescence measurements. The samples were irradiated at 488 nm (FS and OG) and 543 nm (RhB) in a quartz cuvette at room temperature. The dwell time was 0.2 s, and each sample point was scanned twice. Each sample was prepared by adding 10 µL pH nanosensors (50 mg/mL) to 1 mL buffer (0.1M). Fluorescence

emission spectra of the nanosensors at different pH were plotted. From the fluorescence emission spectra of FS, OG and RhB, fluorescence intensity ratios $(IOG+IFS)/IRhB$ were calculated. These fluorescence intensity ratios were then plotted against corresponding pH to obtain the ratiometric pH calibration curves. The triple labelled nanosensor's calibration curve was fitted by the following equation.¹⁵

$$R = \frac{R_1}{10^{pK_{a1}-pH} + 1} + \frac{R_2}{10^{pK_{a2}-pH} + 1} + R_0$$

Where, R is the ratio of emission intensities of the nanosensor. pK_{a1} and pK_{a2} describe the specific pK_a values of the two pH-sensitive fluorophore (OG and FS) conjugated to the SNP. $R_{min} = R_0$ is the ratio for the fully protonated sensor fluorophore and $R_{max} = R_0 + R_1 + R_2$ is the ratio for the fully deprotonated sensor fluorophore.

Characterization

The surface electrostatic property (zeta potential (ζ)) and dynamic light scattering (DLS) measurements were examined with a MALVERN zetasizer ZS90. Zeta potential was measured at 25°C and pH 6; the electrodes were conditioned with KCl aqueous solution (0.5 M) for 200 cycles before measurement. The samples were diluted with Milli-Q water to a final concentration 0.25 mg/mL. Each data point is the average of 3 measurements. The hydrodynamic diameter was measured at room temperature with a fixed scattering angle of 90°. 1.6 mL of pH nanosensors (0.25 mg/mL) in Milli-Q water was subjected to ultrasonic treatment and filtered through a 0.45 μ M needle filter before measurement. Each data point is an average of 3 measurements. Fourier transform infrared spectroscopy (FT-IR) was used to determine the chemical bond status of the samples. FT-IR measurements were performed using KBr pellets on a Nicolet 4700 spectrometer (Thermo Fisher Scientific) in the range of 400-4000 cm^{-1} . The morphology of the nanoparticles was examined using transmission electron microscopy (TEM) with a Hitachi H-7100 microscope. Samples dispersed in ethanol/ Milli-Q water were deposited on carbon-coated Cu grids and dried in air. The fluorescence spectra were measured on a fluorescence spectrophotometer (Hitachi F-4500).

Results and discussion

The Synthesis of pH Nanosensors

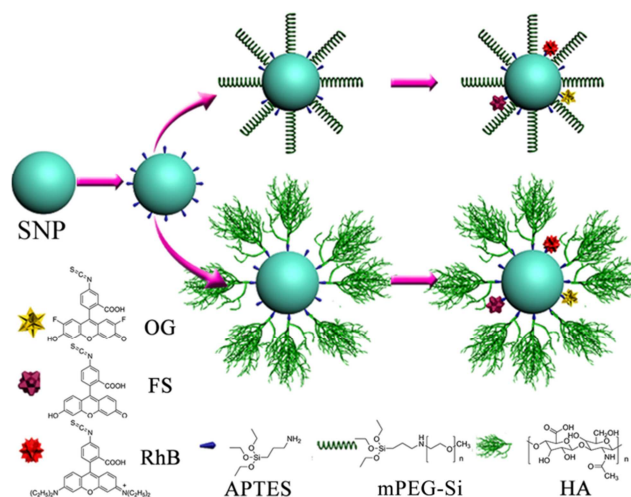


Figure 1 Synthetic Procedure of the sensors.

Figure 1 illustrates the design strategy of the ratiometric nanosensors. The sensor design was based on a SNP core, a functional layer and a polymer shell. SNP were prepared according to Stöber method.³² In some previous reports, amination of SNP was carried out *in situ* at the end of the Stöber synthesis.^{29, 33, 34} The basic condition in the mixture can catalyse the hydrolysis and condensation process. After adding APTES for 2 min, large amount of white precipitate was formed. Even the white precipitate was washed many times with water and ethanol, it was still undispersible. We tried to modify the aggregated particles with PEG. The obtained product is either too big (diameter > 300nm by DLS) or unable to disperse, it seemed that the aggregation between the particles is irreversible. Particle aggregation also has been reported by Buitenhuis, gel permeation chromatography was used in their work to purify the resulted particles.²⁹ However, the complicated purify processing is difficult to achieve in large scale production.

As Figure 2C showed, we supposed at basic pH, the deprotonation of Si-OH ($pK_a=4.8$) would generate negative potential on the local area of SNP surface, whereas the protonation of amino group ($pK_a=11$) would provide a strong positive charge. Consequently, the precipitation of SNP may mainly cause by electrostatic attraction. Once the nanoparticles were precipitated, it was hard to be separated again. To circumvent this problem, ammonium and residual silane oligomers were removed by centrifugation in SNP preparation process. Subsequently, acetic acid was used as catalyst instead of aqueous ammonia to inhibit the deprotonation of Si-OH.

Additionally, the increase of SNP surface charge as the pH decrease (in the range of pH 3-8, Figure S1†) can do a favour for particles dispersion. The investigation of SNP-NH₂ colloidal stability in buffer with varies pH has confirmed our supposition. SNP-NH₂ can be well dispersed in buffer at pH≤6 (Figure 2A and B). When pH was increased to 8, large amount of precipitate has appeared; DLS results indicated the particle aggregation has already started at pH 7. After purification by centrifugation/redispersion cycles, SNP-NH₂ were well dispersed in water at pH 6.

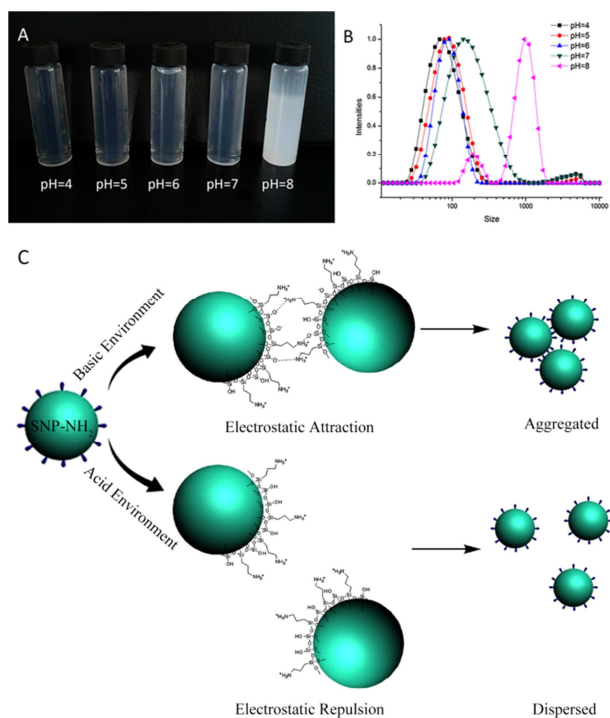


Figure 2 Photographs of SNP-NH₂ dispersed in water at different pH values (A), DLS results of SNP-NH₂ at different pH (B), schematic representation of the SNP-NH₂ aggregation and dispersion in different environments (C).

PEGylation of SNP-NH₂ was carried out by the mixing PEG-silane precursor (Si-PEG) aqueous solution and SNP-NH₂ suspension. The inherent imino groups in Si-PEG could provide a basic environment (about pH 8) to catalyse the condensation reaction. Thus, there was no need to add additional catalyst. After centrifugation/redispersion cycles for several times (5-8 times), the product changed from white dense precipitate to transparent jelly which could be easily dispersed in water under ultrasonic.

In the HA modification, activated HA was added to SNP-NH₂ aqueous suspension (pH=6) directly at first. Unfortunately,

a large amount of flocculated precipitate was formed immediately. After stirring overnight, no particle was observed in the supernatant with DLS measurement. At pH 6, the HA was negatively charged caused by the hydrolysis of carboxyl ($pK_a \approx 2.9$) while the SNP-NH₂ was positively charged.⁴⁰ We concluded that the electrostatic attraction between HA and SNP-NH₂ is the cause of aggregation and precipitation of reaction mixture. Thus, HA coating need to be performed in acidic environment and the pH must be lower than 3 to inhibit the deprotonation of carboxyl from HA. The previously mentioned electrostatic attraction between HA and SNP-NH₂ was reduced. In the following experiments, HCl has been added during the HA functionalization process. Finally, well dispersed HA modified SNP was achieved with diameter 75 nm.

For the further function of fluorophore, two pH sensitive dyes and one reference dye were chosen to expand the measurement range of the sensor and cover the full pH range inside cells. The choice of the pH sensitive dyes, Oregon Green and fluorescein, was based on their respective pK_a values of 4.7 and 6.4. These two dyes are thereby well suited to cover a pH range from approximately pH 4.0–7.5 ($pK_{a \pm 1}$) when combined. Rhodamine B was used as the reference dye.

Material Structural Characterization

Table 1 DLS measurements of nanoparticles (measured at 25°C, pH=6).

Sample	Size(nm)	ζ (mV)	PDI
SNP	31.1±1.2	-24.5±2.7	0.117±0.041
SNP-NH ₂	57.9±2.1	40.8±3.2	0.181±0.062
SNP-HA	72.0±5.0	-25.5±1.8	0.173±0.032
^a SNP-PEG	76.1±3.9	16.8±4.0	0.196±0.016
^b SNP-PEG	102.9±1.0	2.2±0.8	0.194±0.044

^a The amount of PEG used in this sample is 15mg/mL.

^b The amount of PEG used in this sample is 30mg/mL.

The specific surface area of SNP was calculated from the linear part of the Brunauer–Emmett–Teller (BET) plot reached 167 m²g⁻¹ (Table S1† and Figure S2†). Dynamic light scattering (DLS) (Table 1 and Figure 3E) and transmission electron microscope (TEM) (Figure 3) were used for the morphology characterizations of nanoparticles. From the DLS results, the primary SNP was negatively charged (-24.5 mV). It was due to the SiO⁻ group on the particle surface what was generated by

the hydrolysis of Si-OH. After the SNP was functionalized with NH_2 , the particle was positively charged (40.8 mV), which demonstrated that the amine was successfully bounded to SNP. After modified with HA, the zeta potential reversed from 57.9 mV to -25.5 mV, which proved that HA was successfully coated on the nanoparticles. Because the slightly negatively charged PEG can pull down the zeta potential of nanoparticles, the zeta potential (16.8 and 2.2 mV) of SNP-PEG was lower than SNP- NH_2 . The zeta potential (2.2 mV) of high concentration Si-PEG (a) used group was much lower than the low concentration group (b, zeta potential 16.8 mV). Positively charged particles are internalized to a large extent by cells *in vivo* due to electrostatic attraction to the negatively charged cell membrane.²⁶ Besides, it would induce some undesired interaction between the biological environment and the nanocarriers. Polymer modification could effectively reduce the positive potential. From the DLS results, the diameter of nanoparticle SNP and SNP- NH_2 was 31.1 nm and 57.9 nm, respectively. After polymer coating (HA and PEG), the diameter of SNP-HA and SNP-PEG (a) increased to 76.0 and 76.1nm. When increase the dosage of PEG, the size of SNP-PEG (b) increased to 102.9nm.

From the TEM microscopy, we can see that the diameter of SNP (Figure 3A) and SNP- NH_2 (Figure 3B) was 20 and 25 nm, respectively. The TEM image shows the aminated nanoparticles were aggregated, because the pH value of SNP- NH_2 suspension for TEM was 7. After SNP- NH_2 was coated with HA and PEG further, the diameter of SNP-HA (Figure 3C) and SNP-PEG (Figure 3D) increased to 35 nm, which also proved that HA and PEG were successfully bounded to nanoparticles. After surface modified, the shape of all particles (SNP- NH_2 , SNP-HA and SNP-PEG) are more spherical and smoother than SNP. The results of size from DLS were larger than that from TEM. Except for the slight particle aggregation, different principles between these two characterizations are believed to be the main reason for this phenomenon. Generally, DLS studies on the hydrodynamic diameter of nanoparticles whereas TEM observes the morphological specificity of nanoparticles in a dried state. In this study, the hydrodynamic radius of SNP measured by DLS corresponds to the radius of the dense core, plus the thickness of the hydration layer arising from the very hydrophilic PEG and HA in nanoparticles surface. By contrast, TEM only provides the size of the nanoparticles in a dried state

without hydration layer. Similar results have been observed in other works.^{33, 34}

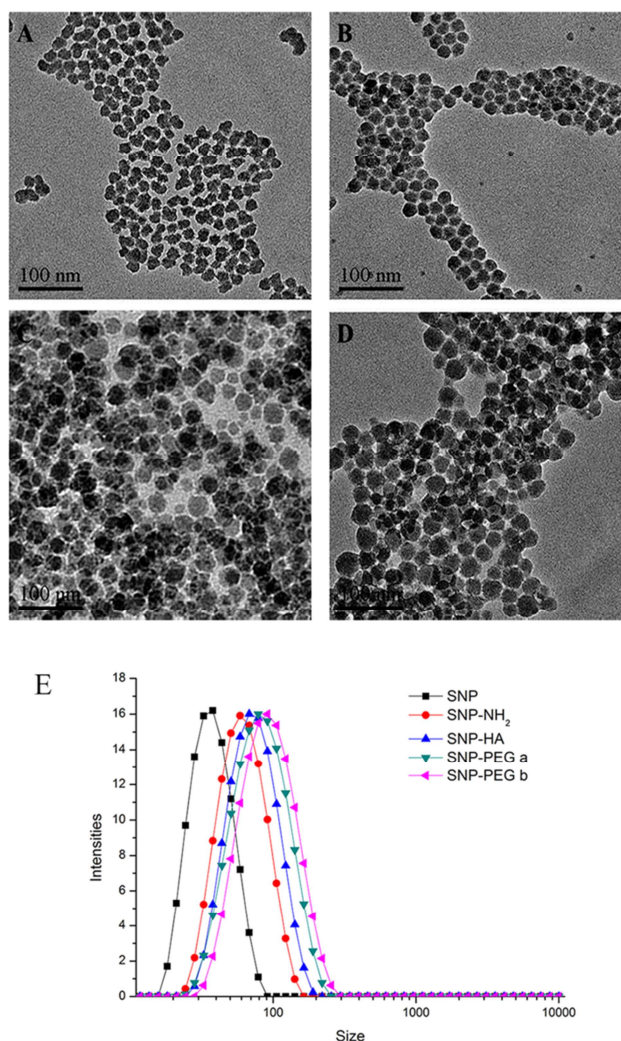


Figure 3 TEM images of SNP (A), SNP- NH_2 (B), SNP- HA (C), SNP- PEG (D) and DLS measurement results (E).

Infrared spectra of all the SNP (Figure 4) show typical bands of the silica framework between 1240 and 1040 cm^{-1} . A broad band at 3600-3100 cm^{-1} is associated with adsorbed water and silanol groups at the surface, the vibration at 1630 cm^{-1} indicates the bending modes of physisorbed water. The vibration at 1560 cm^{-1} indicates amino group have been successfully introduced into the system. The PEG (curve C) and HA (curve D) coated SNP show additional absorption peaks in the range of 2980-2880 cm^{-1} attributed to the C-H stretching modes of the methyl and methylene groups of the polymer chain, respectively. The C-H deformation mode is observed at 1451 cm^{-1} . C-O-C stretching and C-C skeletal vibrations are

covered by the intensive peak of the silica modes in the range of 1260-1100 cm^{-1} . The curve C (SNP-NH₂) shows the carbonyl stretching vibration peak at 1680 cm^{-1} .

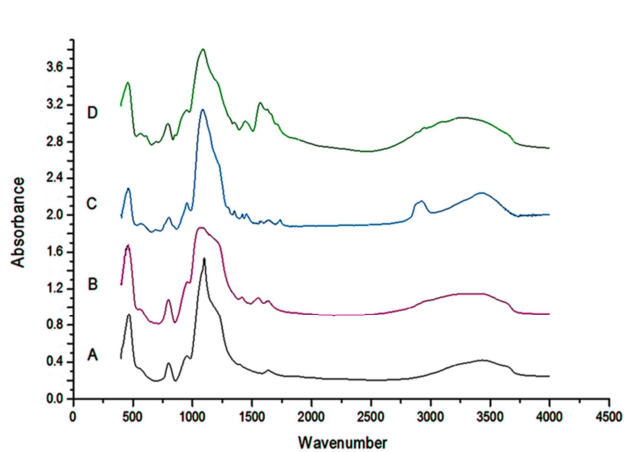


Figure 4 Infrared spectra of silica nanoparticles: SNP (curve A), SNP-NH₂ (curve B), SNP-HA (curve C) and SNP-PEG (curve D).

pH-Sensing Capabilities

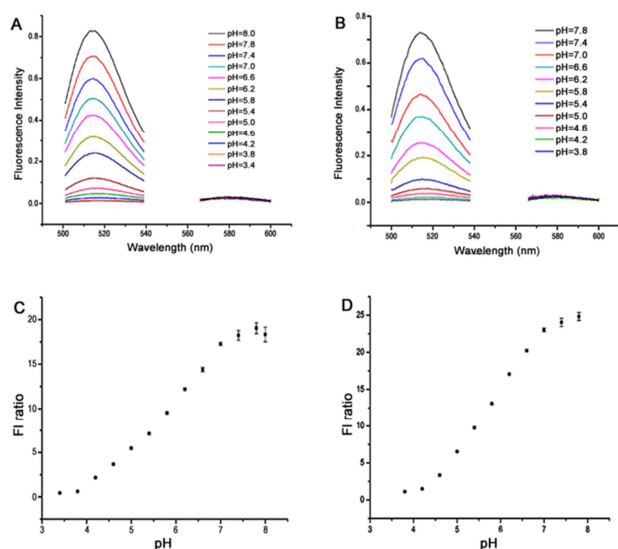


Figure 5 Fluorescence spectra of pH nanosensors at different pH values: SNP-OG-FS-RhB-PEG (A), SNP-OG-FS-RhB-HA (B); Fluorescence intensity ratio (OG+FS)/RhB vs. pH of nanosensors: SNP-OG-FS-RhB-PEG (C), SNP-OG-FS-RhB-HA (D), OG and FS were excited at 488 nm; RhB was excited at 543 nm.

The *in vitro* pH-sensing capabilities of our sensors were determined by fluorescence spectra at different pH values (Figure 5A and B). From the fluorescence emission spectra of the nanosensor fluorescence intensity maxima of pH sensitive fluorophore and reference fluorophore were determined.

(I_{OG+IFS}) represents the maximum emission intensity of the nanosensor when excited at 488 nm and I_{RhB} represents the maximum emission intensity of the nanosensor excited at 543 nm. It showed that the fluorescence intensity of OG and FS increases with pH values, whereas the fluorescence intensities of RhB are relatively constant in the investigated pH interval. Fluorescence intensity ratios (I_{OG+IFA})/ I_{RhB} were plotted against pH to obtain a pH calibration curve (Figure 5 C and D). Even though the polymer coating of the SNP changed their charge greatly, the showed pK_a values of FS and OG were consistent with their theoretical value and only a small change in the pH measurement range was observed. The curves show the sensor SNP-OG-FS-RhB-PEG is sensitive in a pH range from 3.8 to 7.4 (Figure 5C), and the range of sensor SNP-OG-FA-RhB-HA is from pH 4.2 to pH 7.4 (Figure 5D). The reason for this small decrease in measurement range of HA coated sensors is not clear. It is likely that the vast carboxylic groups imported by HA may change the fluorophore local environment slightly.

The Stability Assays

The behavior of the sensors investigated in water and buffer (0.1M, pH range from 3.0 to 7.8) at r.t for up to 3 weeks, with the aim of gaining new insights regarding of these polymer coated pH sensors. The nanoparticles were characterized by DLS which was shown in Table S2[†]. According to the experimental results, polymer coated pH nanosensor showed a remarkable stability in water and buffers. After kept in water for one year at 4°C, the structure of nanoparticles was basically complete and the colloidal stability of sensors was still satisfactory according to the TEM images and DLS results (Figure S4[†] and Figure S5[†]) which were desirable properties for *in vivo* pH measurement.

Conclusions

Preparation of colloidally stable SNP was a challenge due to the particle aggregation. With a simple and effective strategy, polymer coated silica nanoparticles (SNP) with dynamic diameter varied from 76-100nm have been prepared successfully. Three fluorescent dyes were conjugated with SNP via covalent bound to build a ratio metric fluorescence pH sensor, which can minimize the leaching of dyes from nanoparticles. The dynamic pH measurement range was

extended to pH 3.8-7.4 which could cover almost whole physiological conditions, especially the endosomal-lysosomal system. The polymer (methoxypolyethylene glycols and hyaluronic acid) modification offers the nanosensor remarkable colloidal stability which was crucial for living cell measurement. Furthermore, the nanosensors provide a potential way to study SNP internalization process and pH information in cells.

Acknowledgements

The authors would like to thank Kræftens Bekæmpelse and the Danish Research Council for Technology and Production (Grant 274-07-0172), Hubei Province Natural Science Fund Project (2014CFA080, 2014CFB595), National Natural Science Foundation of China (51371079, 81201197, 21401051), Chutian Scholars Fund Project from the Education Department of Hubei Province, and Hundred Talents Program from the Organization Department of Hubei Province for financial support.

References

^a School of Food and pharmaceutical Engineering, Key Laboratory of Fermentation Engineering (Ministry of Education), Hubei Provincial Cooperative Innovation Center of Industrial Fermentation, Hubei University of Technology, Wuhan 430068, China.

*Address correspondence to honghaosuncn@gmail.com.

† Electronic Supplementary Information (ESI) available: [the Specific surface area and nitrogen adsorption/desorption isotherms of SNP; the zeta potentials of SNP-NH₂ at different pH; the stability of Polymer coated nanoparticles in water and buffer; TEM images and DLS results of the sensors after saved in water for 1year]. See DOI: 10.1039/b000000x/

- D. Lagadic-Gossmann, L. Huc and V. Lecureur, *Cell Death Differ.*, 2004, 11, 953–961.
- S. T. Whitten, E. B. García-Moreno and V. J. Hilsner, *Proc. Natl. Acad. Sci. U. S. A.*, 2005, 102, 4282–4287.
- J. R. Casey, S. Grinstein and J. Orlowski, *Nat. Rev. Mol. Cell Biol.*, 2010, 11, 50–61.
- A. Asokan and M. J. Cho, *J. Pharm. Sci.*, 2002, 91, 903–913.
- C. Ju, Ran Mo, and C. Zhang, *Angew. Chem. Int. Ed.*, 2014, 53, 6253–6258.
- W. Huang and D. Yan, *Biomacromolecules*, 2013, 14, 2601–2610.
- J. Pennakalathil and D. Tuncel, *Biomacromolecules*, 2014, 15, 3366–3374.
- C. Bräuchle, and T. Bein, *Chem. Mater.*, 2014, 26, 435–451.
- R. Negrini and R. Mezzenga, *Langmuir*, 2011, 27, 5296–5303.
- R. Bahadur K. C., B. Thapa, and P. Xu, *Mol. Pharmaceutics*, 2012, 9, 2719–2729.
- M. Das and S. Jain, *Mol. Pharmaceutics*, 2013, 10, 3404–3416.
- H. A. Clark, R. Kopelman, R. Tjalkens and M. A. Philbert, *Anal. Chem.*, 1999, 71, 4837–4843.
- H. Sun, K. Almdal and T. L. Andresen, *Chem. Commun.*, 2011, 47, 5268–5270.
- H. Sun, T. L. Andresen, R. V. Benjaminsen and K. Almdal, *J. Biomed. Nanotechnol.*, 2009, 5, 676–682.
- R. V. Benjaminsen, H. Sun, J. R. Henriksen, N. M. Christensen, K. Almdal and T. L. Andresen, *ACS Nano*, 2011, 5, 5864–5873.
- H. Sun, R. V. Benjaminsen, K. Almdal and T. L. Andresen, *Bioconjugate Chem.*, 2012, 23, 2247–2255.
- D. S. Mottram and M. Friedman, *J. Agric. Food Chem.*, 2008, 56, 5983.
- M. Friedman and C. E. Levin, *J. Agric. Food Chem.*, 2008, 56, 6113–6140.
- Veeran M. Chauhan, Gary R. Burnett and Jonathan W. Aylott, *Analyst*, 2011, 136, 1799–1801.
- M. Montalti and L. Prodi, *New J. Chem.*, 2013, 37, 28–34.
- M. S. Moorthy, H. Cho and C. Ha, *Chem. Commun.*, 2013, 49, 8758–8760.
- W. Wu and Y. Tang, *Chem. Commun.*, 2012, 48, 11017–11019.
- H. Meng, J. I. Zink and A. E. Nel, *ACS Nano*, 2010, 4 (8), 4539–4550.
- C. Argyo, C. Bräuchle and T. Bein, *Chem. Mater.*, 2014, 26 (1), 435–451.
- C. Tsou, Y. Hung and C. Mou, *J. Mater. Chem. B*, 2013, 1, 5557–5563.
- E. D. Kirson, V. Dbalý, F. Tovarys, *Proc. Natl. Acad. Sci. USA*, 2007, 104 (24), 10152–7
- W. Lin, Y. Huang, X. Zhou and Y. Ma, *Toxicol. Appl. Pharm.*, 2006, 217, 252–259.
- C. E. Ashley and C. J. Brinker, *Nat. Mater.*, 2011, 10, 389–397.
- V. Cauda, C. Argyo and T. Bein, *J. Mater. Chem.*, 2010, 20, 8693–8699.
- S. Resina and A. R. Thierry, *PLoS One*, 2009, 4(6), e6058.
- Z. Zhang, A. E. Berns, S. Willbold and J. Buitenhuis, *J. Colloid Interface Sci.*, 2007, 310, 446–455.
- W. Stöber, A. Fink, *J. Colloid Interface Sci.*, 1968, 26, 62–69.
- Y. F. Zhu, Y. Fang, L. Borchardt, S. Kaskel, *Microporous Mesoporous Mater.*, 2011, 141, 199–206.
- H. J. Wang, P. Q. Zhao, X. F. Liang, X. Q. Gong, T. Song, R. F. Niu, *J. Chang, Biomaterials*, 2010, 31, 4129–4138.
- H. Hu, H. Zhou and S. Yang, *J. Colloid Interface Sci.*, 2011, 358, 392–398.
- P. Harder, M. Grunze, R. Dahint, G. M. Whitesides and P. E. Laibinis, *J. Phys. Chem. B*, 1998, 102, 426–436.
- J. Groll, E. V. Amirgoulova, G. U. Nienhaus and M. Möller, *J. Am. Chem. Soc.*, 2004, 126, 4234–4239.
- H. Lee, K. Lee and T. G. Park, *Bioconjugate Chem.*, 2008, 19, 1319–1325.
- B. Chang, D. Chen, X. Sha and W. Yang, *Chem. Mater.*, 2013, 25, 574–588.
- H. Lee, K. Lee and T. G. Park, *Bioconjugate Chem.*, 2008, 19, 1319–1325.
- G. Bachar, K. Cohen, and D. Peer, *Biomaterials*, 2011, 32, 4840–4848.
- L. Lapčik, S. De Smedt, J. Demeester and P. Chabreck, *Chem. Rev.*, 1998, 98, 2663–2684.